applied sciences

MDPI

Article

Research on Thermal and Heat Insulation Properties of Aerogel Heat-Insulating Reflective Coatings

Yun-Lin Liu [1,2], Ding-Guo Yang [2], Dong-Hua Wang [2,*] and Xuan Liu [2]

[1] Prefabricated Building Research Institute of Anhui Province, Anhui Jianzhu University, Hefei 230601, China
[2] College of Civil Engineering, Anhui Jianzhu University, Hefei 230601, China
* Correspondence: 500434@ahjzu.edu.cn

Abstract: This study aims to investigate the heat and thermal insulation mechanisms of aerogel heat-insulating reflective coatings. Two working conditions, the hot box method and the open environment at the hot end, were simulated using a gypsum board as the substrate. We conducted thermal tests on blank panels, composite panels with aerogel heat-insulating reflective coatings, and XPS-insulated composite panels for two operating conditions. And the thermal insulation power calculation was carried out for the reflective and barrier materials. The test results show that the air temperature differences between the hot and cold ends of the blank, aerogel coating, and XPS boards under the hot box method were 28.8 °C, 38.2 °C, and 55.2 °C, respectively, and that the air temperature differences between the cold ends of the coating and XPS panels under the natural environment heating condition were 24.2 °C and 24 °C, respectively. Theoretical calculations show that the aerogel heat-insulating reflective coatings produce a net radiative cooling power of 145.9 W/m^2 when the surface of the specimen is at the same temperature as the ambient temperature. The heat flux powers of the aerogel coating board and XPS panel were 9.55 W/m^2 and 1.65 W/m^2 when the temperature difference between the two surfaces on both sides of the specimen was 10 °C, respectively.

Keywords: aerogel heat-insulating reflective coatings; XPS insulation boards; insulation testing; radiant cooling power

check for updates

Citation: Liu, Y.-L.; Yang, D.-G.; Wang, D.-H.; Liu, X. Research on Thermal and Heat Insulation Properties of Aerogel Heat-Insulating Reflective Coatings. *Appl. Sci.* **2023**, *13*, 9700. https://doi.org/10.3390/app13179700

Academic Editor: Shiladitya Paul

Received: 20 July 2023
Revised: 11 August 2023
Accepted: 17 August 2023
Published: 28 August 2023

Copyright: © 2023 by the authors. Licensee MDPI, Basel, Switzerland. This article is an open access article distributed under the terms and conditions of the Creative Commons Attribution (CC BY) license (https://creativecommons.org/licenses/by/4.0/).

1. Introduction

The proportion of energy consumption in the operation phase of buildings to the national total energy consumption is 21.3%, of which heating and air-conditioning energy consumption accounts for 50–70% of the total energy consumption of building operation. Therefore, improving the heat preservation and insulation capacity of building walls is of great significance to realize building energy conservation and promoting the "dual-carbon" strategy [1–3]. Currently, the construction industry mainly uses materials with low thermal conductivity to achieve thermal insulation in buildings [4–7]. But only reducing the thermal conductivity of the wall does not meet the higher demand for building energy efficiency [8,9]. Therefore, some scholars have applied reflective materials to building walls [10,11] to reduce the heat absorption on the wall surface through the reflection effect, as shown in Figure 1a,b for the thermal insulation schematic diagram of barrier materials and reflective materials. Silica aerogel is a strategic cutting-edge new material, and its unique silica chain structure is characterized by high porosity, high reflection, and low thermal conductivity [12,13]. The aerogel heat-insulating reflective coatings (hereafter referred to as aerogel coatings) prepared as functional fillers also have the characteristics of high reflection and low thermal conductivity, which can effectively reduce the heat transfer within the wall. Some scholars [14–17] conducted thermal insulation tests on the prepared aerogel coatings, and the results showed that the aerogel coatings could effectively block heat transfer. However, the research on aerogel coatings focuses more on preparing coatings, and the research on thermal properties needs to be more specific. It cannot be compared effectively with traditional thermal insulation panels.

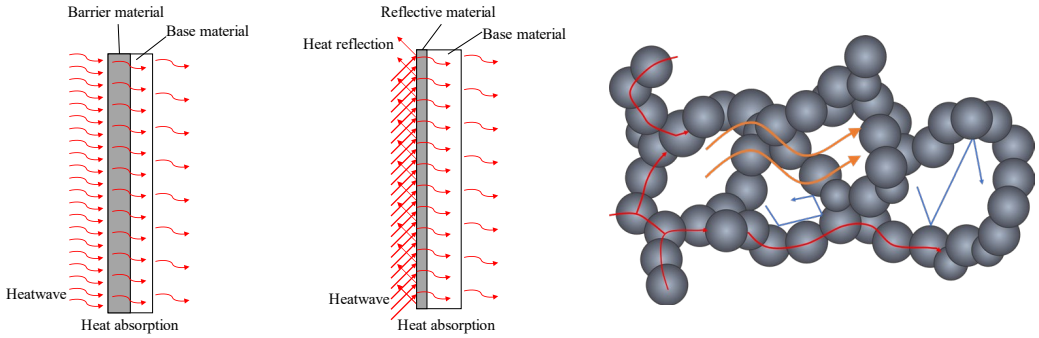


Figure 1. Thermal insulation schematic: (**a**) insulation principle of barrier materials; (**b**) insulation principle of reflective materials; (**c**) insulation principle of aerogel [18].

For this reason, this paper describes study designs of thermal performance comparison tests for thermal insulation boards and aerogel coatings. It explores the enhancement of the thermal insulation performance of building walls by the use of aerogel coatings from the principle of heat transfer calculations. Thermal parameters such as insulation temperature differences, attenuation multipliers, time delays, and the insulation power of the specimens are compared and analyzed.

2. Experimental Studies

2.1. Specimen Preparation

There were three specimens tested in this test; the first board was a 10 mm thick plasterboard coated with a 1 mm thick ordinary white exterior wall coating called blank board; the second board was covered with a 1 mm thick aerogel coating on the surface of the plasterboard following the aerogel coatings' construction process, which is called aerogel board; the third board refers to the external thermal insulation construction practice, using the unique adhesive of Guerch building thermal insulation material to paste the 20 mm thick XPS thermal insulation board on the surface of the plasterboard, called XPS board. XPS is an extruded polystyrene board with the advantages of being lightweight, having low thermal conductivity, and being easy to construct. At present, XPS has been widely used in building exterior wall insulation. We chose XPS boards as a comparison because XPS has a lower thermal conductivity than similar insulation boards and is more accessible for us to cut. Here we need to explain that there are some unavoidable dimensional deviations in the fabrication process of the specimens. Figure 2 shows the designed thickness of each sample, and Table 1 shows the actual measured data of each sample. We will use the actual dimensions for later calculations.

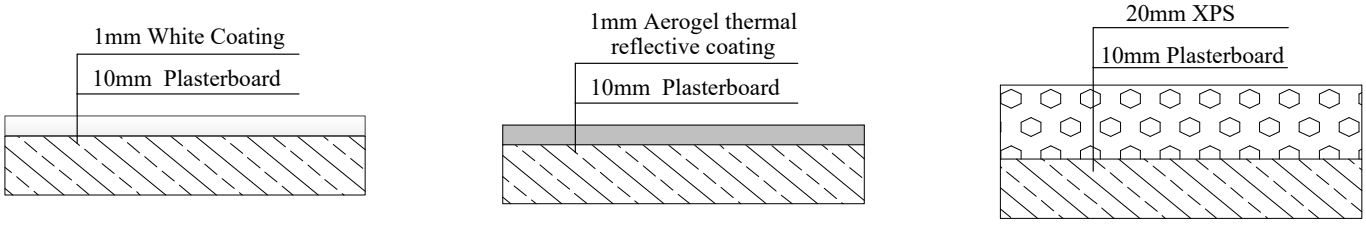


Figure 2. Schematic diagram of the fabrication of each specimen.

2.2. Test Method

Referring to GB/T 13475-2008 and GB/T25261-2018 [19,20], respectively, the test device for the two working conditions shown in Figure 3 was self-made, with working Condition 1 restoring the hot box method and working Condition 2 simulating the natural environmental heating test when the hot end environment is open. The device's walls

were assembled from 65 mm thick XPS insulation panels, and the joints were sealed using construction insulation adhesive and a combination of insulating aluminum foil tape. In Condition 1, the test piece was placed in the middle of the chamber, and the section was divided into two parts. On one side, a 275 W infrared heating lamp was recognized as the heat source for the hot end and the other was the cold end. In Condition 2, one side of the chamber wall was replaced by the test piece to be tested. An infrared lamp was positioned 30 cm above the test piece to heat it. The air conditioning maintained a test environment temperature of (20 ± 1) °C. As shown in Figure 3, four T-type thermocouples were arranged on both sides of the test piece to collect the surface temperature of the test piece, while thermocouples were placed on each side of the test piece to manage the air temperature at the hot and cold ends, and for Condition 2 a thermocouple was arranged 2 m away from the device to collect the ambient room temperature. On the surface of the specimen, four thermocouples were located at right angles to a square with a side length of 270 mm, the center of which was the center of the specimen. Every 5 min, the DH3818Y collected the temperature with an accuracy of ±0.2 °C. The temperature inside the testing chamber was only affected by the heat source because the insulation capacity of the tested sample was much lower than that of the walls. The temperature change between the two adjacent thermocouples during the heating and cooling phases should not exceed 0.2 °C to be considered a steady state. Based on the pretest results, the heating time for the test was set to 400 min.

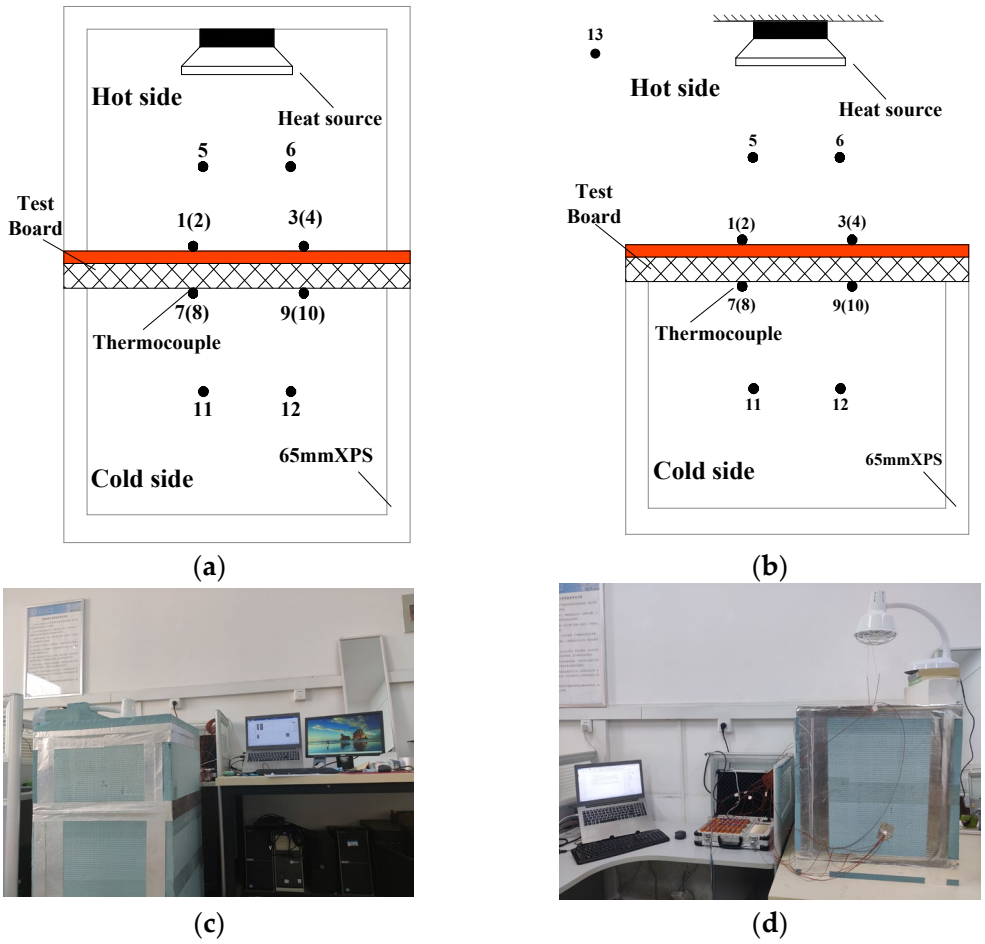


Figure 3. Diagram of the test setup: (**a**) diagram of Condition 1 test; (**b**) diagram of Condition 2 test; (**c**) physical view of Condition 1 test; (**d**) physical view of Condition 2 test.

Table 1. Table of test piece material parameters.

Materials	Thickness mm	Thermal Conductivity W/(m·K)	Manufacturers
Plasterboard	9.7	0.120	Hefei Youtai Building Materials Co. Hefei, China
Aerogel coatings	1.1	0.066	Laboratory homemade
XPS insulation panels	19	0.037	Nanjing Ogle Energy Saving and Environmental Protection Technology Co. Nanjing, China
White coating	1	0.117	Anhui Xin Peng New Material Co. Anqing, China

3. Data Analysis

3.1. Temperature of the Measuring Point for Condition 1

Figure 4 shows the temperature change curves of the three specimens in working Condition 1. Recent findings suggest that all three shared a similar pattern of temperature fluctuation, consisting of specific periods of warming and cooling. According to Figure 4a–c, the infrared heat source lamp significantly impacted the air temperature inside the hot end and the surface temperature of the test piece at the hot end. The air temperature at the cold end and the surface temperature of the specimen at the stern end have a more moderate trend than at the hot end, indicating that the presence of the model effectively blocks the heat transfer between the cold and hot ends [21,22]. We compared the surface temperature trends at the hot end and the air temperature at the hot end of the three specimens during the warming stage; as shown in Figure 4a–c, the temperature curves' slopes at the specimen's hot end at 10 min were 1.25, 2.28 and 4.65 for the blank, aerogel, and XPS boards, respectively. The slopes of the air temperature curves at the hot end of the three specimens at 10 min were 2.38, 3.15, and 4.25, respectively. This indicates that the XPS board formed the most effective insulation against heat under the same conditions. The heat not transferred to the cold end gathered in the hot end space, so the air temperature at the hot end was higher for the better-insulated specimens. After turning off the heat source, both the sample's surface temperature and the hot end's air temperature experienced a sudden and noticeable decrease. There was a significant time delay in the air temperature change at the cold end because the specimen blocked the heat transfer between the cold and hot ends. The slopes of the curves for the aerogel and blank boards were the same when the temperature was reduced, as seen in Figure 4d, indicating that the aerogel coatings did not significantly improve the thermal insulation performance of the substrate.

3.2. Temperature of the Measuring Point for Working Condition 2

The temperature of the test specimen was lower than the temperature of the test specimen in Condition 1, and the temperature of the test specimen was lower than that of the test specimen in Condition 2. By comparing Figure 5a–c, we can see that during the heating stabilization stage, the surface temperature of the XPS board was 36 °C at the heat source side of the test piece, which was much higher than the surface temperature of the other two test pieces. This suggests that the XPS board's surface absorbs more heat. The surface temperature of the hot end was the lowest as the aerogel coatings reflected most of the heat. Figure 5d shows the air temperature curves in the cold box for the three specimens and shows that the fastest temperature rise was for the blank board, followed by the aerogel board, and the slowest was for the XPS board. The temperatures of the XPS board and the aerogel board were 24 °C and 24.2 °C, respectively, during the stabilization phase. From the heat insulation point of view, 1 mm aerogel coatings can achieve the same effect as a 2 cm XPS insulation board. The slopes of the temperature curves of the three specimens with a temperature of 22.5 °C in the cooling stage were taken for comparison due to the different initial cooling temperatures. When the temperature dropped to 25 °C,

the slopes of the curves were −0.065, −0.053, and −0.034 for the blank, aerogel, and XPS board, respectively. This shows that the XPS board has better thermal insulation properties than the aerogel board.

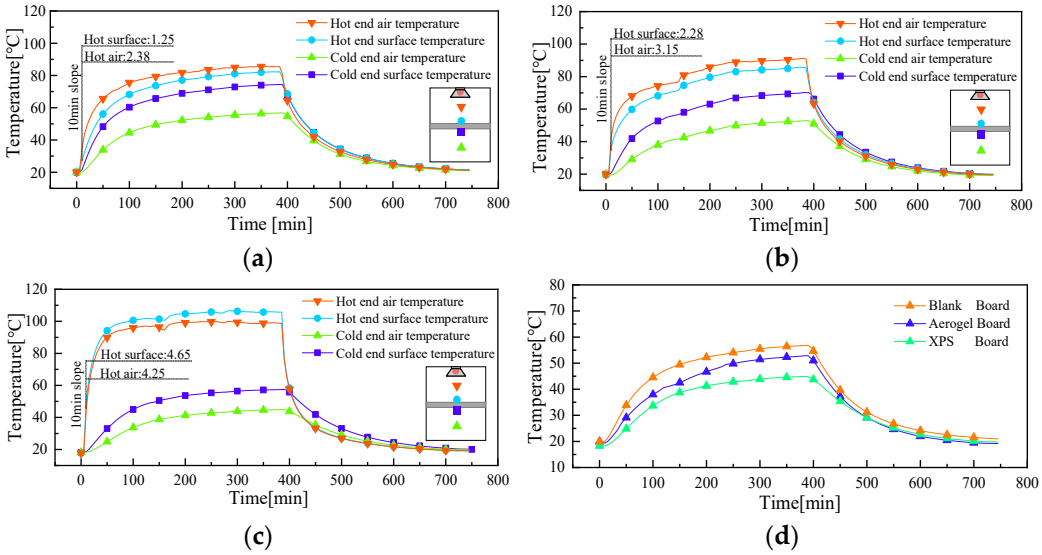


Figure 4. Temperature variation curves of test pieces for working Condition 1: (**a**) blank board temperature variation; (**b**) aerogel board temperature variation; (**c**) XPS board temperature variation; (**d**) cold side air temperatures of three specimens.

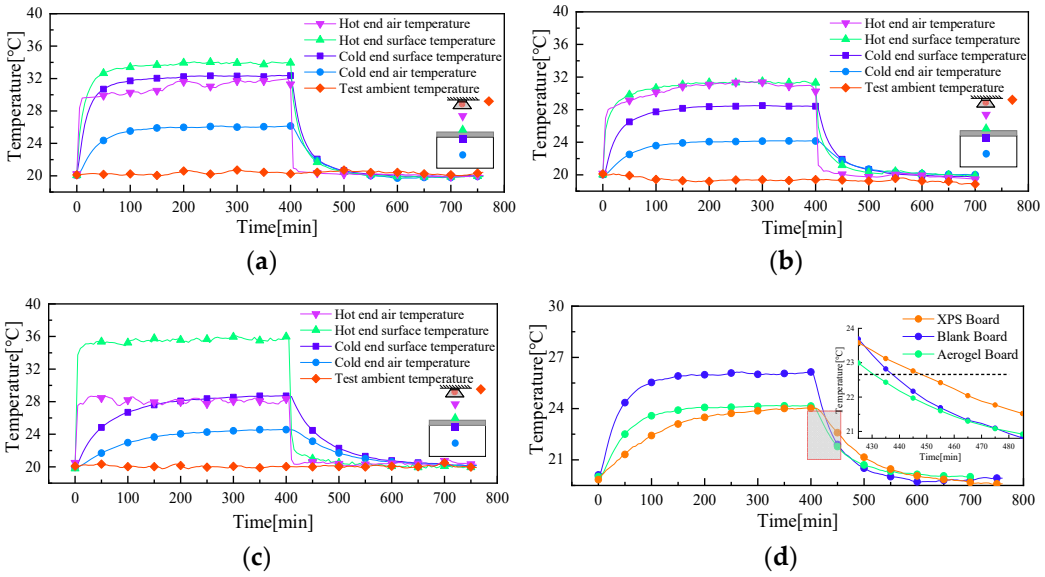


Figure 5. Temperature variation curves of test piece for working Condition 2: (**a**) blank board temperature variation; (**b**) aerogel board temperature variation; (**c**) XPS board temperature variation; (**d**) cold side air temperature of three specimens.

3.3. Characteristic Data Analysis

As defined in the Code for Thermal Design of Civil Buildings [23], the decay multiplier and time delay were calculated for all three samples. The time delay and decay multiplier reflect the thermal storage capacity of the material. A material's thermophysical properties and thickness determine its different time delays and decay multipliers. A high time delay and low attenuation multiplier for a building wall indicate that the wall has excellent thermal storage capacity. When the external environment fluctuates to a certain extent, a wall with a high time delay and low attenuation multiplier can ensure a stable indoor temperature. The Thermal Design Code for Civil Buildings expresses the formula for both.

Table 2 presents data comparing the thermal insulation performances of blank specimens with aerogel and XPS boards under two working conditions.

$$\mathrm{f} = \frac{T_{cold}^{max} - T_{cold}^{min}}{T_{hot}^{max} - T_{hot}^{min}} \tag{1}$$

$$\varnothing = t_{cold}^{max} - t_{hot}^{max} \tag{2}$$

where f is the damping factor, T_{cold}^{max} is the maximum value of the ambient temperature in the cold box, T_{cold}^{min} is the minimum value of the ambient temperature in the cold box, T_{hot}^{max} is the maximum value of the ambient temperature in the hot box, and T_{hot}^{min} is the minimum value of the ambient temperature in the hot box; $\varnothing$ is the time log, t_{hot}^{max} is the time corresponding to the time when the ambient temperature inside the hot box reaches its maximum value, and t_{cold}^{max} is the time corresponding to the time when the ambient temperature in the cold box reaches its maximum value.

Table 2. Calculation of damping factor and time lag of specimens.

Test Conditions	Feature Data	Blank Board	Aerogel Board	XPS Board
Test Condition 1	Damping factor	0.560999743	0.469470229	0.323897396
	Time lag/min	20	25	140
Test Condition 2	Damping factor	0.553571429	0.368421053	0.459770115
	Time lag/min	5	40	360

During the heating phase of Condition 2, fluctuations in the test data curve occurred due to the influence of the test environment on the air temperature at the hot end. In Condition 2, errors may have arisen in calculating the decay multiplier and time delay because of data points with the same temperature value. This is documented in reference [24]. The calculation results for Condition 1 show that the XPS insulation board increased the time delay of the blank board by a factor of seven, which is of great significance in maintaining a stable room temperature. From the data, it can be concluded that the thermal insulation efficacy of the aerogel coating is far from that of the XPS insulation board. Still, it is worth noting that the thickness of the aerogel coating is 1 mm. In contrast, the thickness of the XPS insulation board is 2 cm, thus showing that the application of aerogel coating to the insulation and thermal insulation of building facades will be a disruptive development. Comparing the calculated decay multiplier and time delay results for the aerogel and XPS boards, it has been discovered that the use of aerogel coating has a minimal impact on the thermal insulation capability of the blank board. The effect of XPS on the blank boards was more intuitive, as it related to the thickness of the test specimens, the test environment, and the material properties [25]. The decay multiplier and time delay, in combination with the temperature change curve and the temperature difference distribution in the final steady state, also confirm the different specimen insulation capacities from another perspective.

Figure 6 shows the temperature field distribution of each specimen during the warming and stabilization phase. The closed hot box test conditions increased the hot end temperature by 60 °C compared to the open test conditions. The XPS board showed excellent thermal insulation and heat preservation performance in working Condition 1, making the air temperature difference between the cold and hot ends 55.2 °C, much higher than the 38.2 °C of the aerogel board. The air temperature difference between the hot and cold ends of the XPS board was 4.7 °C, which was lower than that of the blank board at 5 °C. This indicates that the reflectivity of the aerogel coatings allowed the heat transferred by the infrared lamp to be reflected into the test environment, reducing the amount of heat passing through the specimen. The open hot end environment was conducive to the reflective properties of the aerogel coatings, effectively reducing the amount of heat passing through the specimen. It is worth noting that the XPS board had the most significant temperature difference between the sample's hot and cold ends in Condition 2, as the XPS board surface

absorbs more heat, resulting in a higher surface temperature. The temperature difference between the hot and cold ends of the specimens under both conditions was the smallest for the blank plate, followed by the aerogel board, and the largest was for the XPS board. It can be seen that the efficiency of heat transfer in the XPS board is the lowest; aerogel coating does not take into account reflectivity, and the aerogel coating itself also has a specific function of blocking heat transfer, but the amount is lower than that of the XPS board.

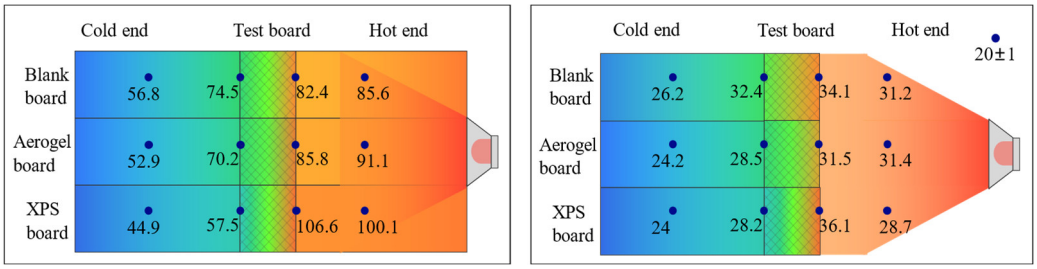


Figure 6. Emperature field distribution of the specimen during the stable heating stage: (**a**) temperature field distribution diagram under Condition 1; (**b**) temperature field distribution diagram under Condition 2.

4. Theoretical Heat Transfer Calculations

The results of the tests phenomenologically characterized the thermal insulation performances of aerogel coatings and XPS insulation boards. Quantitatively comparing the thermal insulation efficiencies of reflective and barrier materials from a computational point of view has been a difficulty in academic research and engineering applications [26]. Therefore, we measured the aerogel coatings' solar reflectance and vertical emissivity, and that of ordinary white exterior wall coatings. We also calculated the radiant heat-blocking power of the two coatings. And, we also combined the thermal conductivity of aerogel coating and XPS insulation board to calculate the barrier heat transfer power of the two materials.

4.1. Calculation of Radiant Heat Transfer

The heat involved in a coating consists of four components [27–29], the thermal radiation q_{rad} emitted outward by the coating itself, the heat q_{sun} radiated by the sun to the specimen, the heat q_{air} released by the surrounding atmosphere to the surface of the sample, and the heat loss q_{loss} generated outward by the sample itself. Hence, the total power of the coating to radiate the heat insulation can be expressed as follows:

$$q_{re} = q_{rad} - q_{sun} - q_{air} - q_{loss} \tag{3}$$

$$q_{rad} = \int \varepsilon(\lambda) I_b(\lambda, T_s) \mathrm{d}\lambda \tag{4}$$

$$q_{sun} = \int \varepsilon(\lambda) I_{\mathrm{sun}}(\lambda) \mathrm{d}\lambda \tag{5}$$

$$q_{air} = \int \varepsilon(\lambda) I_{air}(\lambda) \mathrm{d}\lambda \tag{6}$$

$$q_{loss} = H(T_{air} - T_s) \tag{7}$$

where $\varepsilon(\lambda)$ is the spectral emissivity of the specimen; $I_b(\lambda, T_s)$ is the blackbody radiative force at different wavelengths for a blackbody at a temperature of T_s.; $I_{\mathrm{sun}}(\lambda)$ is the standard AM1.5 solar spectrum; $I_{air}(\lambda)$ is the ambient radiative force, calculated from $I_{air}(\lambda) = \varepsilon_{air}(\lambda) I_b(\lambda, T_{air})$; $\varepsilon_{air}(\lambda)$ is the atmospheric transmittance, $I_b(\lambda, T_{air})$ is the temperature for the T_{air} equivalent blackbody radiative force; H is the integrated radiative heat

transfer coefficient of the coating surface; T_{air} and T_s are the ambient temperature around the specimen and the specimen surface temperature, respectively; the related calculation plots are shown in Figure 7.

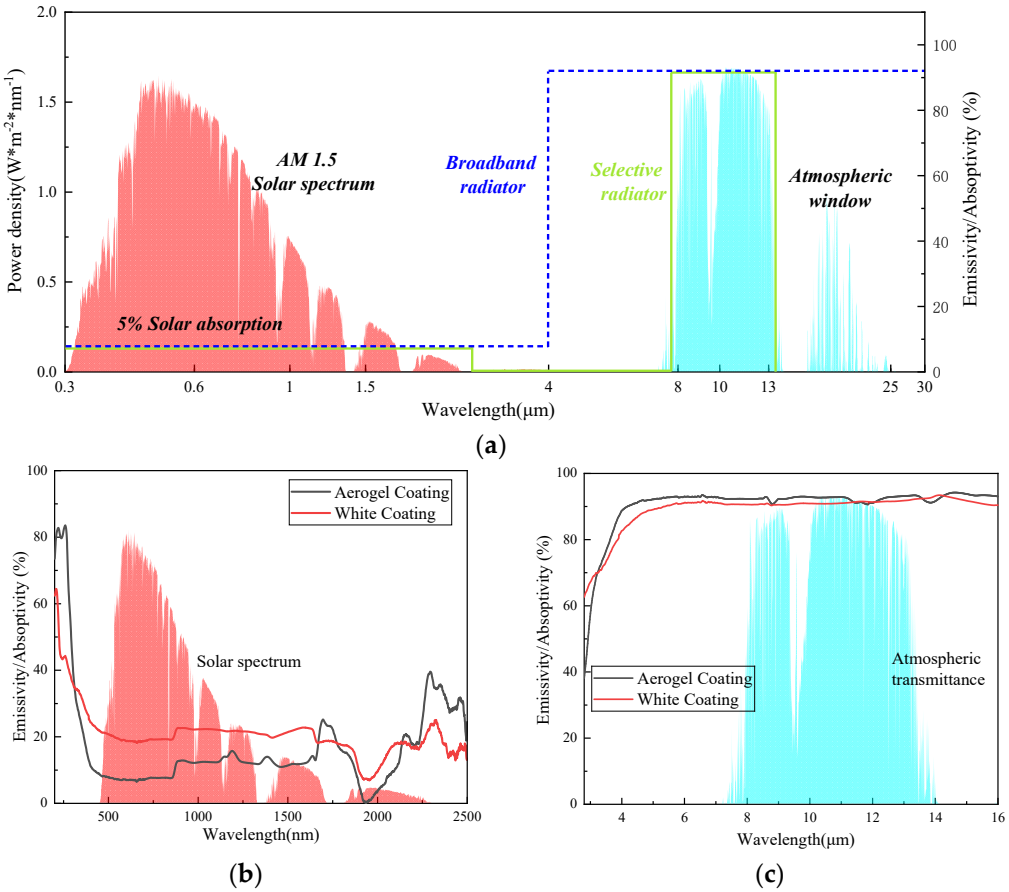


Figure 7. Plot of radiant power calculation. (**a**) Schematic diagram of radiant power calculation [27,30,31]; (**b**) standard solar spectrograms and coatings' solar spectral absorption diagrams; (**c**) graph of atmospheric transmittance and infrared emissivity of coatings.

Figure 7a shows the absorptivity and emissivity of an ideal radiative cooling material in different wavelength bands. We want the coatings to have lower absorption in the solar radiation band (250–2500 nm) and higher emissivity in the atmospheric window (7–14 μm). We tested the absorptivity and emissivity of the aerogel coating and white coating in the corresponding bands, as shown in Figure 7b,c. The test results show that the aerogel coatings have lower absorption than white coatings in 300–1500 nm wavelengths. However, the emissivity of the two coatings is very close in the 7–14 μm wavelength. This shows that the aerogel coatings have better radiative cooling ability in the visible and near-infrared wavelengths. The total power, q_{sun}, of solar radiation energy absorbed by aerogel coatings and ordinary facade coatings was calculated to be 102.7 W/m^2 and 206.2 W/m^2. It has been shown [29] that ideal radiatively cooled materials have high emissivity in the wavelength range of ≥4 μm, and the leading radiant energy bands in the atmospheric window are 7–14 μm. Therefore, we integrated only 7–14 μm in calculating the q_{air} and figured that the aerogel coatings and ordinary facade coatings receive atmospheric radiant powers of 117.4 W/m^2 and 115.8 W/m^2. The intensities of atmospheric radiation received by the aerogel coating and the regular exterior coating were calculated to be 117.4 W/m^2 and 115.8 W/m^2. Similarly, because the integration band of q_{rad} is also 7–14 μm, the calculation results of the aerogel coating and white exterior wall coating were 366.1 W/m^2 and 370.6 W/m^2, respectively. When the coating surface was at the same temperature as the ambient temperature (q_{loss} = 0 W/m^2), the net radiant

insulation powers of the aerogel coating and the white exterior coating were obtained as 145.9 W/m^2 and 48.6 W/m^2. This shows that the reflective and heat-insulating ability of the aerogel coating is fully demonstrated, and our test results also show that the hot end surface temperature of the aerogel boards was lower than that of the blank boards and XPS boards under the same conditions.

4.2. Calculation of Heat Transfer Barrier

The equivalent thermal resistance value is currently an essential index for evaluating the thermal performance of building materials. According to Fourier's law of heat conduction, the heat transfer power of a one-dimensional single-layer wall can be simplified as Equation (8), and the equivalent thermal resistance value can be used to calculate the heat transfer power within a multi-layer wall for composite walls composed of multi-layer materials. The thermal resistance value of single-layer materials is calculated by Equation (9), and the equivalent thermal value is the sum of the thermal resistance values of each layer. To be able to compare the heat transfer power of aerogel board and XPS board, it was assumed that the temperature difference between the two sides of the wall was 10 °C ($T_1 - T_2$ = 10 °C). The contribution of the coating primer and XPS board binder to the equivalent thermal resistance value was ignored in the calculations; the materials of each layer are tightly bonded to each other, and the temperature of the two fabrics on the bonding surface was the same. The rest of each calculation parameter is shown in the previous Table 1, and the calculation results are shown in Table 3.

$$q = \frac{T_1 - T_2}{R} \tag{8}$$

$$R_i = \frac{\mathrm{d}_i}{\lambda_i} \tag{9}$$

$$R = \sum R_i \tag{10}$$

where T_1 and T_2 are the temperatures on both sides of the wall, inside and outside; R_i and R are the single-layer wall's thermal resistance value and the equivalent thermal resistance value of the multi-layer composite wall; and d_i and λ_i are the thickness of each layer of the wall and the coefficient of thermal conductivity.

Table 3. Calculation of heat transfer power.

	R_i K/W				R K/W	q W/m^2
	Plasterboards	**Aerogel Coating**	**White Coating**	**XPS**		
Blank board	0.81	/	0.10	/	0.91	10.98
Aerogel board	0.81	0.24	/	/	1.05	9.55
XPS board	0.81	/	/	5.14	5.94	1.68

Calculation results show that the aerogel coating has a significant radiative cooling ability compared with the white wall coating due to the aerogel material's high reflective properties. When the temperature difference between the two surfaces of the specimen is assumed to be fixed, the aerogel coating does not show its high reflective properties, and it relies on its internal porous structure to block heat transfer as traditional thermal insulation materials do. The thermal conductivity of our aerogel coating was higher than that of the XPS insulation board, and the thickness of the coating was so thin that the heat flow density through the aerogel board was 7.87 W/m^2 higher than that of the XPS board. Therefore, the temperature difference between the hot and cold ends of the XPS board should be significantly higher than that of the blank and aerogel boards, which is consistent with the results of our tests.

5. Conclusions

Simulating two working conditions for thermal testing of plasterboard, aerogel board, and XPS board, the temperature distribution curves of the specimens under the two working conditions were obtained. The following conclusions can be drawn by analyzing the temperature change curves and characteristic data and combining them with the calculated values of radiative cooling thermal power and barrier thermal power.

Under Condition 1 and Condition 2 conditions, the aerogel board can enlarge the air temperature difference between the hot and cold ends by 32.6% and 44% compared with the blank board. From the data curve of the thermal insulation test, the thermal insulation ability of a 20 mm thick XPS board is more robust than that of a 1 mm thick aerogel coating. Still, the high reflective property of aerogel coating in Condition 2 makes the surface temperature of the hot end of the aerogel board significantly lower than that of the remaining two samples. The heat transfer efficiency calculations show that the radiative cooling power of the aerogel coating is 145.9 W/m2, and the radiative insulation power of the white coating is 48.6 W/m2, which increases the cooling efficiency by two times. When the temperature difference between the two sides of the sample is 10 °C, 1 mm aerogel coating can reduce the heat transfer of plasterboard by 1.42 W/m2 (>10%), and the heat transfer of 20 mm XPS by 9.33 W/m2, but their thicknesses differ by 20 times. This is of great significance to the energy-saving design of building facades.

Author Contributions: Conceptualization, writing—review and editing, Y.-L.L.; writing—original draft preparation, and methodology, Y.-L.L. and D.-G.Y.; validation, D.-H.W. and D.-G.Y.; project administration, Y.-L.L., D.-H.W. and X.L.; supervision, Y.-L.L.; All authors have read and agreed to the published version of the manuscript.

Funding: This research was funded by the University Natural Science Research Project of Anhui Province (CN), grant number KJ2020ZD43, KJ2021A0607, 2022AH050261; Anhui Housing Urban-Rural Development Scientific and Technological projects (2022-RK057); the Anhui Jianzhu University Doctoral Initiation Fund (2020QDZ17, 2022QDZ23).

Institutional Review Board Statement: Not applicable.

Informed Consent Statement: Not applicable.

Data Availability Statement: Not applicable.

Conflicts of Interest: The authors declare that they have no known competing financial interests or personal relationships that could have appeared to influence the work reported in this paper.

References

1. Qian, D.; Li, Y.; Niu, F.; O'Neill, Z. Nationwide savings analysis of energy conservation measures in buildings. *Energy Convers. Manag.* **2019**, *188*, 1–18.
2. Ibrahim, M.; Bianco, L.; Ibrahim, O.; Wurtz, E. Low-emissivity coating coupled with aerogel-based plaster for walls' internal surface application in buildings: Energy saving potential based on thermal comfort assessment. *J. Build. Eng.* **2018**, *18*, 454–466.
3. Makar, M.; Pravica, L.; Kutija, M. Supercapacitor-Based Energy Storage in Elevators to Improve Energy Efficiency of Buildings. *Appl. Sci.* **2022**, *12*, 7184.
4. Li, C.L.L. Experimental study of the thermal performance of a building wall with vacuum insulation panels and extruded polystyrene foams. *Appl. Therm. Eng. Des. Process. Equip. Econ.* **2020**, *180*, 115801.
5. Malunjkar, G.; McElroy, H.; Coroneo, M.; Ogunniyi, A.O. Improving the quality of rigid polyurethane foam sandwich insulation panels. *MRS Adv.* **2023**, *8*, 489–493. [CrossRef]
6. Vaidya, A.; Uddin, N.; Vaidya, U. Structural characterization of composite structural insulated panels for exterior wall applications. *J. Compos. Constr.* **2010**, *14*, 464–469. [CrossRef]
7. Thai, H.N.; Kawamoto, K.; Nguyen, H.G.; Sakaki, T.; Komatsu, T.; Moldrup, P. Measurements and Modeling of Thermal Conductivity of Recycled Aggregates from Concrete, Clay Brick, and Their Mixtures with Autoclaved Aerated Concrete Grains. *Sustainability* **2022**, *14*, 2417. [CrossRef]
8. Lakatos, Á.; Csík, A. Multiscale Thermal Investigations of Graphite Doped Polystyrene Thermal Insulation. *Polymers* **2022**, *14*, 1606.
9. Vitale, M.; Cascone, S.M. Thermal, Physical and Mechanical Performance of Orange Peel Boards: A New Recycled Material for Building Application. *Sustainability* **2021**, *13*, 7945.

10. Zhang, G.; Wu, H.; Liu, J.; Yang, J.; Huang, H.; Ding, Y.; Xie, L. Dynamic performance and energy efficiency of reflective and insulative composite coating on building exterior wall. *Build. Simul.* **2022**. [CrossRef]
11. Karim, A.N.; Johansson, P.; Kalagasidis, A.S. Knowledge gaps regarding the hygrothermal and long-term performance of aerogel-based coating mortars. *Constr. Build. Mater.* **2022**, *314*, 125602.
12. Calisesi, M. Aerogel Incorporated Plasters and Mortars the Case Study of Precast Panels. Diploma Thesis, Alma Mater Studiorum—Università di Bologna, Bologna, Italy, 2016.
13. Ganesamoorthy, R.; Vadivel, V.K.; Kumar, R.; Kushwaha, O.S.; Mamane, H. Aerogels for water treatment: A review. *J. Clean. Prod.* **2021**, *329*, 129713.
14. Buratti, C.; Moretti, E.; Belloni, E.; Agosti, F. Development of Innovative Aerogel Based Plasters: Preliminary Thermal and Acoustic Performance Evaluation. *Sustainability* **2014**, *6*, 5839–5852.
15. Di, Z.; Ma, S.; Wang, H.; Guan, Z.; Lian, B.; Qiu, Y.; Jiang, Y. Modulation of Thermal Insulation and Mechanical Property of Silica Aerogel Thermal Insulation Coatings. *Coatings* **2022**, *12*, 1421.
16. Patricia Fernanda Bergmann, B.; Carmeane, E.; Adilson, S. Lightweight thermal insulating coating mortars with aerogel, EPS, and vermiculite for energy conservation in buildings. *Cem. Concr. Compos.* **2021**, *125*, 104283. [CrossRef]
17. Carnicer, V.; Canas, E.; Orts, M.J.; Sánchez, E. Feasibility of incorporating silica aerogel in atmospheric plasma spraying coatings. *Ceram. Int.* **2021**, *18*, 47.
18. Eunyoung, K.; Kit-Ying, C.; Jie, Y.; Venkatesan, H.; Adegun, M.H.; Zhang, H.; Lee, J.-H.; Shen, X.; Kim, J.K. Engineering anisotropic structures of thermally insulating aerogels with high solar reflectance for energy-efficient cooling applications. *J. Mater. Chem. A* **2023**, *11*, 7105–7114.
19. Wang, J.; Petit, D.; Ren, S. Transparent thermal insulation silica aerogels. *Nanoscale Adv.* **2020**, *2*, 5504–5515.
20. *ISO 8990:1994*; General Administration of Quality Supervision, Inspection and Quarantine of the People's Republic of China. Thermal Insulation—Determination of Steady-State Thermal Transmission Properties—Calibrated and Guard Hot Box. China National Standardization Administration: Beijing, China, 1994; p. 24.
21. *GB 25261-2018*; State Administration of Market Administration. Solar Heat Reflecting Insulation Coatings for Buildings. China National Standardization Administration: Beijing, China, 2018; p. 24.
22. Yun, T.S.; Jeong, Y.J.; Han, T.S.; Youm, K.S. Evaluation of thermal conductivity for thermally insulated concretes. *Energy Build.* **2013**, *61*, 125–132. [CrossRef]
23. Ropelewski, L.; Neufeld, R.D. Thermal inertia properties of autoclaved aerated concrete. *J. Energy Eng.* **1999**, *125*, 59–75.
24. *GB 50176-93*; Thermal Design Code for Civil Building. National Standards of the People's Republic of China: Beijing, China, 2015; pp. A90–A94.
25. Zhao, Z.; Yang, X.; Qu, X.; Zheng, J.; Mai, F. Thermal insulation performance evaluation of autoclaved aerated concrete panels and sandwich panels based on temperature fields: Experiments and simulations. *Constr. Build. Mater.* **2021**, *303*, 124560.
26. Fathipour, R.; Hadidi, A. Analytical solution for the study of time lag and decrement factor for building walls in climate of Iran. *Energy* **2017**, *134*, 167–180.
27. Streimikiene, D.; Skulskis, V.; Balezentis, T.; Agnusdei, G.P. Uncertain multi-criteria sustainability assessment of green building insulation materials. *Energy Build.* **2023**, *219*, 110021.
28. Zhao, B.; Hu, M.; Ao, X.; Chen, N.; Pei, G. Radiative cooling: A review of fundamentals, materials, applications, and prospects. *Appl. Energy* **2019**, *236*, 489–513.
29. Xue, X.; Qiu, M.; Li, Y.; Zhang, Q.M.; Li, S.; Yang, Z.; Feng, C.; Zhang, W.; Dai, J.-G.; Lei, D. Creating an Eco-Friendly Building Coating with Smart Subambient Radiative Cooling. *Adv. Mater.* **2020**, *32*, 42.
30. Available online: https://download.csdn.net/download/Diamond4058/16809577 (accessed on 3 April 2023).
31. Available online: https://www.gemini.edu/bserving/telescopes-and-sites/sites#Transmission (accessed on 17 December 2022).

Disclaimer/Publisher's Note: The statements, opinions and data contained in all publications are solely those of the individual author(s) and contributor(s) and not of MDPI and/or the editor(s). MDPI and/or the editor(s) disclaim responsibility for any injury to people or property resulting from any ideas, methods, instructions or products referred to in the content.